Model Skill and Sensitivity for Simulating Wave Processes on Coral Reefs Using a Shock-Capturing Green-Naghdi Solver

Edward Beetham, Paul S Kench, Stéphane Popinet

Journal of Coastal Research

Model Skill and Sensitivity for Simulating Wave Processes on Coral Reefs Using a Shock-Capturing Green-Naghdi Solver

--Manuscript Draft--

Manuscript Number:	
Full Title:	Model Skill and Sensitivity for Simulating Wave Processes on Coral Reefs Using a Shock-Capturing Green-Naghdi Solver
Short Title:	Analysis of Green-Naghdi model skill on coral reefs
Article Type:	Research Article (Professional Paper)
Keywords:	wave transformation; Green-Naghdi; model sensitivity; phase-resolving model; infragravity waves; wave setup; runup
Corresponding Author:	Edward Paul Beetham, PhD University of Auckland Auckland, Auckland NEW ZEALAND
Corresponding Author Secondary Information:	
Corresponding Author's Institution:	University of Auckland
Corresponding Author's Secondary Institution:	
First Author:	Edward Paul Beetham, PhD
First Author Secondary Information:	
Order of Authors:	Edward Paul Beetham, PhD
	Paul Simon Kench, PhD
	Stéphane Popinet, PhD
Order of Authors Secondary Information:	
Abstract:	Wave flume data from published benchmark experiments were used to extensively evaluate numerical model skill and sensitivity for applying a shock-capturing Green-Naghdi (GN) model to simulate nonlinear wave transformation processes on complex coral reefs. Boussinesq-type models that utilise nonlinear shallow water equations (NSWEs) to represent wave breaking and dissipation hold significant potential for understanding coastal hazards associated with global environmental change and sea-level rise. These fully nonlinear phase-resolving models typically require a threshold condition to switch from dispersive equations to shock-capturing NSWEs in areas of active wave breaking. However, limited information exits regarding how this splitting approach influences the behaviour of different surf-zone processes that contribute to wave runup and inundation on coral reefs. This paper presents a comprehensive analysis of model sensitivity to explore how input parameters that control wave breaking and dissipation influence the behaviour of sea-swell (SS) waves, infragravity (IG) waves, wave setup, runup and solitary waves on coral reefs. Results show that each wave process exhibits unique sensitivity to the free-surface slope threshold (B) that is used to represent areas of active wave breaking by locally switching from the weakly-dispersive GN equations to the shock-capturing NSWEs. However, accurate representation of all wave processes can be achieved if the wave-face steepens to at least 35 degrees ($B \geq 0.7$) before breaking is initiated. Results from this research support and encourage the use of nonlinear phase-resolving wave models as tools for academic research, coastal management, coastal engineering and hazard forecasting on atoll and fringing reef environments.
Suggested Reviewers:	Ryan Lowe ryan.lowe@uwa.edu.au Specialist in wave modeling on coral reefs
	Robert Brander

	rbrander@unsw.edu.au Specialist in wave processes on coral reefs
	Cyprien Bosserelle cyprienb@spc.int Specialist in numerical modeling wave processes coral reefs
Opposed Reviewers:	

Dear Editor,

We are pleased to submit our article titled Model Skill And Sensitivity For Simulating Wave Processes On Coral Reefs Using A Shock-Capturing Green-Naghdi Solver to be considered for publication in the Journal of Coastal Research. This research paper presents a comprehensive review of model behaviour, skill and sensitivity for simulating nonlinear wave processes on coral reefs in high resolution. Our hope is that this paper opens the door for scientists, managers and engineers to use nonlinear phase-resolving models to examine the impacts of future environmental change to coral reef landforms.

We have prepared all figures in greyscale to suit publication in print and online and have no conflicts of interest.

Regards
Eddie Beetham
School of Environment,
University of Auckland

Model Skill and Sensitivity for Simulating Wave Processes on Coral Reefs Using a Shock-Capturing Green-Naghdi Solver

Edward Beetham[†]*, Paul S Kench[†], and Stéphane Popinet[‡]

[†]School of Environment, University of Auckland, New Zealand

***corresponding author: e.beetham@auckland.ac.nz**

[‡]Sorbonne Universités, UPMC Univ Paris 06, CNRS, UMR 7190, Institut Jean Le Rond d'Alembert, F-75005 Paris, France

ABSTRACT

Wave flume data from published benchmark experiments were used to extensively evaluate numerical model skill and sensitivity for applying a shock-capturing Green-Naghdi (GN) model to simulate nonlinear wave transformation processes on complex coral reefs. Boussinesq-type models that utilise nonlinear shallow water equations (NSWEs) to represent wave breaking and dissipation hold significant potential for understanding coastal hazards associated with global environmental change and sea-level rise. These fully nonlinear phase-resolving models typically require a threshold condition to switch from dispersive equations to shock-capturing NSWEs in areas of active wave breaking. However, limited information exits regarding how this splitting approach influences the behaviour of different surf-zone processes that contribute to wave runup and inundation on coral reefs. This paper presents a comprehensive analysis of model sensitivity to explore how input parameters that control wave breaking and dissipation influence the behaviour of sea-swell (SS) waves, infragravity (IG) waves, wave setup, runup and solitary waves on coral reefs. Results show that each wave process exhibits unique sensitivity to the free-surface slope threshold (B) that is used to represent areas of active wave breaking by locally switching from the weakly-dispersive GN equations to the shock-capturing NSWEs. However, accurate representation of all wave processes can be achieved if the wave-face steepens to at least 35 degrees ($B \geq 0.7$) before breaking is initiated. Results from this research support and encourage the use of nonlinear phase-resolving wave models as tools for academic research, coastal management, coastal engineering and hazard forecasting on atoll and fringing reef environments.

ADDITIONAL INDEX WORDS: *wave transformation, Green-Naghdi, model sensitivity, phase-resolving model, infragravity waves, wave setup, runup.*

INTRODUCTION

Coral reefs are characterised by a steep sloping offshore fore-reef that quickly transitions into a shallow and near-horizontal reef flat. This abrupt transition results in energetic wave breaking at the reef edge, where approximately 86% of incident wave energy is dissipated (Ferrario *et al.*, 2014). Wave energy is further dissipated through friction on the reef flat, with up to 97% reduction of incident wave energy by the shoreline (Ferrario *et al.*, 2014). The rate of dissipation through breaking and friction are both influenced by reef depth, leading to consistent measurements of tidally modulated wave heights at the shoreline (Kench and Brander, 2006). The dependence of shoreline wave height on reef depth means that sea-level rise (SLR) is expected to increase wave energy impacting reef fringed landforms, resulting in widespread flooding and coastal erosion within the 21st century (Storlazzi *et al.*, 2015). However, incident wave attenuation on coral reefs is associated with a transfer of energy to free-propagating infragravity waves (Péquignet, Becker, and Merrifield, 2014; Pomeroy *et al.*, 2012) and an increase in reef flat water level through wave setup (Becker, Merrifield, and Ford, 2014; Vetter *et al.*, 2010). The behaviour of these secondary wave motions on coral reefs is not comprehensively understood and this knowledge gap presents a significant limitation for process based management and engineering on reef coastlines facing SLR. The significance of these secondary wave motions is evident in the fact that all documented cases of wave overtopping on reef landforms identify infragravity waves as the primary process contribution to flooding (Cheriton, Storlazzi, and Rosenberger, 2016; Ford, Becker, and Merrifield, 2013; Roeber and Bricker, 2015; Shimozono *et al.*, 2015).

Accurate modeling of wave transformation processes, swash dynamics, runup and overtopping on coral reefs landforms is critical for understanding the physical vulnerability of reef coastlines facing SLR and environmental change (Reyns *et al.*, 2013). However, for models to be an effective hazard management tool, they must accurately represent all the

nonlinear wave transformation processes that influence runup and inundation (Roeber and Bricker, 2015). Previous attempts to model the impact of SLR on reef landforms (*e.g.* Storlazzi *et al.*, 2015, Storlazzi *et al.*, 2004) rely on phase-averaging techniques that oversimplify energy transfer from incident waves to secondary surf-zone processes and do not simulate high frequency water level motions associated with SS waves, runup or overtopping. Recently, Roeber and Bricker (2015) show that phase-averaging models typically used in coastal hazard assessments do not resolve nonlinear energy transfers in the surf-zone or wave generated flooding. A 'free-surface' or phase-resolving model is required to directly simulate all surf-zone processes, runup and overtopping motions.

Coral reef morphology creates an inherent challenge for applying phase-resolving wave models because there is a rapid transition from dispersion dominant processes on the fore-reef slope to flux dominant processes at the reef edge (Fang, Liu, and Zou, 2016; Roeber and Cheung, 2012b). The first challenge is to propagate waves through the shoaling zone in a way that captures the asymmetrical transformation in wave shape and height prior to breaking (Huntley, 2013). The second challenge is to resolve wave breaking processes in a way that represents wave shape, dissipation and the generation of secondary wave motions (Roeber and Cheung, 2012b). To overcome these challenges, recent advances have focused on developing fully nonlinear Boussinesq-type solvers that apply 'shock-capturing' techniques to locally represent wave breaking using nonlinear shallow water (NSW) equations (Bonneton *et al.*, 2011a; Bonneton *et al.*, 2011b; Lannes and Marche, 2015; Popinet, 2015; Roeber and Cheung, 2012b; Tissier *et al.*, 2012a). A number of recent studies have shown that shock-capturing Boussinesq-type models can represent incident wave shoaling, breaking and attenuation on coral reefs, while also replicating the generation of infragravity waves and wave setup (Beetham *et al.*, 2016; Fang, Liu, and Zou, 2016; Roeber and Cheung, 2012b; Shimozono *et al.*, 2015; Su, Ma, and Hsu, 2015). These studies are all based on different solutions for the

Boussinesq and NSW equations and collectively highlight the capability of phase-resolving models to simulate nonlinear wave processes on complex coral reef environments. Each of these models also applies a threshold condition for wave instability that is used to locally and temporarily switch from dispersive equations to shock-capturing equations in areas of active wave breaking. Complex techniques for switching between source terms include: a momentum gradient threshold (Roeber and Cheung, 2012b); a Froude number threshold (Su, Ma, and Hsu, 2015); and a wave height to water depth threshold (Shimozono *et al.*, 2015). However, the simplest approach that represents how wave breaking is physical triggered is a threshold free-surface slope (Beetham *et al.*, 2016; Bonneton *et al.*, 2011b; Fang, Liu, and Zou, 2016; Popinet, 2015). Regardless of the method, the threshold value chosen to initiate wave breaking has a significant influence on breakpoint location and therefore directly influences the generation and behaviour of secondary wave processes. However, the exact sensitivity of different surf-zone processes to wave breaking parameterisation remains unknown.

The aim of this research is to quantify the sensitivity of different surf-zone processes that contribute to wave runup and overtopping on coral reefs to the parameters that influence wave breaking and dissipation in the open source Green-Naghdi model from Popinet (2015). The Green-Naghdi (GN) equations are a large amplitude solution of the Boussinesq equations which makes them particular suitable to coastal reef environments (Fang, Liu, and Zou, 2016). With the growing application of shock-capturing Boussinesq-type models on coral reef environments, it is important for users to understand how threshold values chosen to initiate wave breaking influence the full spectrum of wave transformation processes. This paper presents results form a comprehensive sensitivity analysis of how the free-surface slope threshold value (B) influences SS wave dissipation, IG wave behaviour, setup magnitude, runup elevation and solitary wave dynamics on morphologically complex coral reefs. The combined influence from friction is accounted for by testing the sensitivity of B when

combined with different friction coefficient (C_f) values. A series of published benchmark scenarios were used to undertake this analysis, including: include irregular wave transformation on a 2D reef (Demirbilek, Nwogu, and Ward, 2007); solitary wave interaction with a 2D reef (Roeber and Cheung, 2012b); and solitary wave interaction with a 3D reef (Lynett *et al.*, 2011).

METHODS

This research uses the shock-capturing Green-Naghdi model developed by Popinet (2015) to simulate laboratory scale scenarios of wave interaction with coral reefs. The Green-Naghdi solution is an attractive option for coral reefs because the weakly-dispersive equations can be applied to relatively large amplitude waves $\left(a/h_o \sim 1\right)$ propagating across nontrivial variations in topography $\left(B_z/h_o \sim 1\right)$, where a is the characteristic wave amplitude, h_o is water depth and B_z is the topographic gradient (Popinet, 2015). These characteristics provide a fully nonlinear solution of wave behaviour in shallow water, but are limited to weakly-dispersive scenarios relatively close to the shoreline $\left(h_o^2/L_o^2 \ll 1\right)$, where L_o is the offshore wave length (Bonneton *et al.*, 2011b, Lannes and Marche, 2015, Popinet, 2015). For a description of the governing equations and numerical scheme of the model used in this paper, the reader is referred to Popinet (2015) or the Basilisk website (Popinet, 2014), where the documented source code and a series of examples are freely available.

Wave Breaking

The weakly-dispersive finite-difference solver for wave propagation and shoaling is locally removed in areas of wave breaking, allowing wave shape and dissipation to be solved with a finite-volume solution of the NSW equations (Popinet, 2015). Similar approaches to represent wave breaking are becoming increasingly popular in a new generation of shock-

capturing GN models (Bonneton *et al.*, 2011a; Bonneton *et al.*, 2011b; Lannes and Marche, 2015; Popinet, 2015; Tissier *et al.*, 2012a; Tissier *et al.*, 2012b). In Popinet (2015), the weakly dispersive GN equations are used unless the local free-surface slope $\left(\|\nabla\eta\|\right)$ exceeds a user defined threshold (B), which by default is 1 (45°). At each time-step, on all cells where $\|\nabla\eta\| > B$ is true (as calculated by the GN equations), the dispersive function is locally deactivated and the finite volume NSW solution is applied to resolve wave shape and dissipation throughout the breaking process. Therefore, the dispersion equations may be re-applied shoreward of the breakpoint if reef flat water depth can accommodate broken wave heights to a point that the free-surface slope decreases below the B threshold. This is important for accurately propagating reformed wave energy across the reef flat, at which point friction becomes the main form of dissipation. For the simulations presented here, an implicit quadratic bottom friction term (1) was included as:

$$\boldsymbol{S}_f = -C_f \,\|\boldsymbol{u}\|\,\boldsymbol{u}, \tag{1}$$

where C_f is a non-dimensional coefficient that influences the rate of dissipation across the reef flat.

Application to Coral Reefs

Shock-capturing GN models have been used to simulate wave transformation, infragravity waves and setup on laboratory scale (Fang, Liu, and Zou, 2016) and field scale (Beetham *et al.*, 2016) coral reefs. Simulations presented in Beetham *et al.* (2016) show that the GN model from Popinet (2015) can accurately represent field scale wave transformation processes. However, the Popinet (2015) model has yet to be evaluated against benchmark data for wave runup and overtopping on coral reefs. Therefore, the Popinet (2015) GN model was used in this research to provide a new and comprehensive evaluation of the model skill and

158 sensitivity for simulation nonlinear wave transformation processes, runup and overtopping
159 processes on a range of coral reef environments. Such benchmarking is required for confidently
160 using the model as a research and coastal hazard management tool.

161 A visual description of how the shock-capturing GN model represents wave processes
162 on coral reefs is presented in Figure 1, in the context of irregular wave transformation on an
163 idealised reef morphology. This example highlights how the shock-capturing scheme is
164 implemented near the reef edge to produce an asymmetrical wave bore profile on the outer reef
165 flat, characterised by a vertical face and gradual tail. Figure 1 also highlights how incident
166 wave attenuation is associated with setup of mean water level on the reef flat (Figure 1a) and a
167 distinct transfer of energy into the IG wave band (Figure 1d-e). This example shows that
168 maximum wave runup elevation is a function of remnant SS wave energy, IG wave oscillations
169 and wave setup.

170 **Outline of Test Cases**

171 Benchmark test one (BM1) simulated wave transformation processes across a 'typical'
172 Guam fringing reef (Figure 2a) from the University of Michigan (UM) wind wave flume
173 experiment presented by Demirbilek, Nwogu, and Ward (2007). The UM experiment was
174 initially undertaken to evaluate the Boussinesq model by Demirbilek and Nwogu (2007), and
175 has subsequently become a standard benchmark for applying wave models to coral reef
176 environments (*e.g.* Buckley, Lowe, and Hansen, 2014; Demirbilek and Nwogu, 2007;
177 Demirbilek, Nwogu, and Ward, 2007; Filipot and Cheung, 2012; Nwogu and Demirbilek,
178 2010; Sheremet *et al.*, 2011; Shimozono *et al.*, 2015; Su, Sheremet, and Smith, 2011; Zijlema,
179 2012). Here, the Popinet (2015) GN model was evaluated against fifteen incident scenarios
180 from the UM dataset. The model was used in 1D, with measured water level from wave gauge
181 1 (WG1) imported as the wave boundary condition. Model outputs for SS wave height (H_{ss}),

IG wave height (H_{ig}), wave setup ($\overline{\eta}$) and maximum runup (R_{max}) were compared with flume data to assess model accuracy and sensitivity. A comprehensive sensitivity analysis was undertaken to identify how systematic variations in B and C_f influence each output parameter (H_{ss}, H_{ig}, $\overline{\eta}$ and R_{max}). Results presented below identify the B and C_f combinations that best represents the range of processes across the surf and swash zone, out of 14 C_f values and 8 B values (112 combinations) for the 15 test conditions (1,680 simulations). Pressure sensor data from the wave flume experiment were retrieved from http://cirp.usace.army.mil/pubs/techreports.php.

Benchmark test two (BM2) simulated a solitary wave breaking on an emerged 1D reef crest using nine combinations of B and C_f. These nine combinations were chosen because they represent the most sensitive and most accurate values form BM1. Data obtained during the Hawaii reef (HI reef) experiment from the O.H. Hinsdale Wave Research Laboratory at Oregon State University presented in Roeber and Cheung (2012) were used to evaluate model results. The HI reef test simulated a 0.75 m solitary wave breaking on an emerged reef crest, with water plunging into and propagating across a shallow lagoon (Figure 2b). BM2 tested numerical representations of dispersion, nonlinearity, wave breaking, overtopping and wet/dry dynamics (Roeber and Cheung, 2012b). Bathymetry and water level data from the wave flume experiment were downloaded from http://hydraulic.lab.irides.tohoku.ac.jp/app-def/S-102/2014/?page_id=56.

Benchmark test three (BM3) was taken from the National Tsunami Hazard Mitigation Program benchmarking repository (NTHMP, 2012). BM3 simulated a solitary wave interacting with a complex 3D shelf that has a triangular extension and an emerged conical island (Figure 2c), from the flume experiments by Lynett *et al.* (2011). BM3 used the GN model in 2D (depth averaged) and required solutions for dispersion, shoaling, refraction, diffraction, breaking,

206 overtopping and wet/dry dynamics. The 3D shelf experiment has become a popular Boussinesq
207 model benchmark scenario (Fang *et al.*, 2013; Shi *et al.*, 2012; Roeber and Cheung, 2012a;
208 Yamazaki *et al.*, 2012) with bathymetry and wave gauge data available online
209 (http://coastal.usc.edu/currents_workshop/problems.html). The same nine combinations of C_f
210 and B from BM2 were tested again in BM3.

211 **Output Data Analysis**

212 For BM1, time-series data for free-surface water level from the UM wave flume and
213 numerically modeled water level outputs at each WG location were analysed using the same
214 techniques. Simulations ran for 900 s, with mean depth across the platform stabilising after
215 approximately 100 s of wave activity. Data were extracted at 20 Hz (consistent with flume
216 experiment) and trimmed to only include the final 700 s of wave activity when the wave field
217 was developed across the reef. A spectral filter with a 0.25 Hz (4 s) cut-off was used to separate
218 SS and IG wave components. The 0.25 Hz separation is approximately double the peak incident
219 wave period used in the wave basin experiments. Significant wave heights for SS (H_{ss}) and IG
220 (H_{ig}) components were then calculated using a zero down-crossing routine in Matlab. Wave
221 setup ($\bar{\eta}$) was calculated as the mean free-surface displacement. Wave spectra were calculated
222 from the raw pressure signal using the first 8192 samples from t = 200 s, with an overlapping
223 hamming window and 16 degrees of freedom. Maximum runup (R_{max}) was calculated from
224 numerical model outputs using profile data for maximum water level across the reef flat. R_{max}
225 values reported in Demirbilek and Nwogu (2007) were used to evaluate numerical model
226 outputs.

227 Model skill was used to quantify how close numerical outputs were to wave flume
228 measurements in all benchmark tests using equation (2), where P_i is the model value, O_i is the
229 wave flume value and vertical bars indicate absolute values.

$$\text{Skill} = 1 - \frac{\sum\left|(P_i - O_i)^2\right|}{\sum\left(\left|P_i - \overline{O}\right| + \left|O_i - \overline{O}\right|\right)^2} \quad (2)$$

A skill value of one indicates a perfect match between predicted and observed data and a skill value of zero indicates that there is no agreement between the predicted and the observed (Lowe *et al.*, 2009). Model skill was calculated individually for each wave statistic (H_{ss}, H_{ig}, setup, runup) in BM1. Mean skill averaged across these output parameters was then used to understand overall model accuracy and sensitivity for representing wave processes at the shoreline. For BM2 and BM3, model skill was calculated using time-series data for the free-surface water elevation, from numerical and wave flume outputs at each wave gauge location.

RESULTS

This section describes the results from each of the benchmark tests and presents a comprehensive analysis of model behaviour on coral reefs. Collectively, these results identify values for B and C_f that are suitable for accurately simulating nonlinear wave transformation processes, runup and overtopping on coral reef environments.

Benchmark Test 1: Wave Transformation and Runup

Model outputs from BM1 show that the shock-capturing GN equations are capable of replicating flume measurements of SS wave height, IG wave height, setup and runup with maximum model skill between 0.90 and 0.99 (Table 1). This section outlines the sensitivity of each individual wave process to variations in B and C_f and identifies values that provide the most accurate representation of all wave processes at the shoreline, including runup elevation.

Model Sensitivity to the Breaking Slope Threshold (B)

The breaking slope threshold influences the water depth where wave breaking is triggered and determines whether waves break on the reef slope, reef edge or reef flat. The B

value therefore influences the rate and mode of incident wave dissipation which has implications for IG wave behaviour and the magnitude of wave setup on the reef flat. Maximum model skill for H_{ss} at the shoreline was 0.90, achieved using B = 0.4 (Figure 3a; Table 1). However, skill = 0.89 was achieved using B values between 0.4 and 1.2, indicating that a range of values can be used to predict shoreline wave height (Figure 3a). Model outputs for H_{ss} at the shoreline (WG9) were consistently higher using B = 0.4, with a slight decrease in skill and wave height observed when B increased from 0.4 to 0.7 (Figure 3a; Figure 4a-i). However, H_{ss} values were highly variable using these lower B values, with 11% difference in outputs between B = 0.4 and B = 0.7. In comparison, consistent outputs for H_{ss} were achieved using higher B values (0.7-1.2), characterised by 0.9% variation (Table 1). Overall, maximum skill was associated with B = 0.4 but high skill and minimum sensitivity were achieved for H_{ss} using $B \geq 0.7$, especially when combined with $C_f \leq 0.008$.

Infragravity waves were highly sensitive to B, with a 16.7% difference between minimum and maximum values for H_{ig} at the shoreline (Figure 3b; Table 1). Interestingly, this range decreased dramatically to only 1% variability between H_{ig} outputs using $B \geq 0.7$. IG wave height at the shoreline was highest using B = 0.4, with a linear decrease in H_{ig} observed as B increased to 0.7 and consistent outputs between B = 0.7-1.2 (Figure 4a-i). However, maximum model skill (0.98) for shoreline H_{ig} was achieved across a range of B values between 0.4 and 0.8 (Figure 3b). Lower B slopes achieved maximum skill when combined with high friction, compared to higher B values generating maximum skill across a range of low and moderate friction values (Figure 3b). Overall, it was possible to achieve high model skill using all B values (depending on friction) but IG behaviour was highly variable using $B \leq 0.6$, compared to consistent H_{ig} predictions with minimal sensitivity associated with $B \geq 0.7$ (Figure 3b).

Model outputs for setup magnitude at WG9 were highest using B = 0.4, with a 15.1% decrease in setup observed between B = 0.4 and B = 0.7. Higher B values (≥0.7) produced consistent setup magnitudes, with minimal variation between B = 0.7 and B = 1.2. Low B values over-predicted setup and were associated with a 7.5% decrease in model skill. The increase in setup using low B values explains why H_{ig} and H_{ss} were highest and often over-predicted using $B \leq 0.6$. Maximum skill for wave setup (0.99) was achieved using B = 1 but skill above 0.98 was achieved across a wide range of friction values when combined with $B \geq 0.7$ (Figure 3b).

Maximum runup elevation is influenced by the magnitude of H_{ss}, H_{ig} and setup at the shoreline. Therefore, model outputs for R_{max} reflect the combined sensitivity of all surf-zone processes. H_{ss}, H_{ig} and setup were all largest using B = 0.4, which resulted in significantly over-predicted wave runup outputs (Figure 4j-r) and low skill (Figure 3e), unless unrealistically high friction values were used. Maximum R_{max} skill (0.94) was achieved using B = 0.7 (combined with C_f = 0.01), with peak skill for most friction coefficients associated with B = 0.7. Runup skill above 0.92 was achieved across a range of B values between 0.6 and 1.2, with higher friction required to produce accurate runup results when combined with low B values. Runup elevation was 20% lower (on average) and much closer to flume measurements when using $B \geq 0.7$.

Model Sensitivity to Friction Coefficient

Quadratic bottom friction has a direct influence on wave attenuation across the model domain and has a significant impact on SS and IG wave transmission across the reef flat. Maximum model skill for H_{ss} (0.90) was associated with C_f = 0.004, with wave heights typically over-predicted using lower values and under-predicted using higher values (Figure 4a-i). SS waves were reasonably sensitive to C_f, with an average 14.6% decrease in shoreline H_{ss} observed as C_f increased from 0.001 to 0.01 (Table 1). Friction values above 0.01 resulted

300 significantly under-predicted wave heights (Figure 4) and a substantial decrease in skill (Figure
301 3a). Maximum model skill for H_{ig} was achieved with C_f = 0.006 (0.98), but skill > 0.95 was
302 achieved across a range of C_f values between 0.002 and 0.008 (Figure 3b). IG waves were
303 highly sensitive to C_f, with an average 23.2% decrease in shoreline H_{ig} as C_f increased from
304 0.001 to 0.01. IG wave transmission across the reef flat was highly influenced by C_f, with low
305 friction resulting in shoreward amplification and high friction resulting in shoreward
306 dissipation. Friction had no influence on wave setup, with only 0.7% variability between
307 outputs and skill > 0.98 achieved by all C_f values (Figure 3c). Wave runup was highly sensitive
308 to C_f, with a 31% decrease in R_{max} observed when C_f increased from 0.001 to 0.01 (Table 1).
309 R_{max} was typically over-predicted using $C_f \leq 0.06$ and under-predicted using $C_f \geq 0.02$, with
310 close predictions of flume runup and high skill (>0.92) achieved using C_f = 0.005 – 0.01 (Figure
311 4j-r). Runup results reflect how SS waves and IG waves respond to friction, with low friction
312 associated with slightly larger SS waves and significantly larger IG wave heights at the
313 shoreline. Runup sensitivity to C_f is primarily associated with how friction influences IG wave
314 transmission across the reef flat.

315 **Maximum Shoreline Skill**

316 Model skill values calculated for each individual wave processes were most consistent when
317 using higher B values (0.7 - 1.2) with moderate friction (C_f = 0.002 - 0.008). To quantify the
318 accuracy and sensitivity of surf-zone processes, mean skill at WG9 was calculated by averaging
319 skill values for H_{ss}, H_{ig} and setup. The best representation of all wave processes at WG9 (mean
320 skill = 0.95) was achieved using B = 0.8 and C_f = 0.003, with skill > 0.94 associated with all B
321 values between 0.6 and 1.2 combined with C_f between 0.001 and 0.006 (Figure 3d). Wave
322 processes at WG9 were highly sensitive to low B values, with a 14% decrease in the sum
323 amplitude of H_{ss}, H_{ig} and setup between B = 0.4 and B = 0.7. Higher B values produced
324 consistent outputs with less than 1% variation between B = 0.7 and B = 1.2. Output sensitivity

to low B values was most pronounced for IG waves (17%) and setup (16%), with SS waves observing slightly less variation (12%). Overall, model skill at WG9 was higher and outputs were more consistent when using B values between 0.7 and 1. Increasing friction from 0.001 to 0.01 had no impact on setup but did force a linear decrease in SS and IG wave height at WG9 (Figure 4). Friction had a major influence on IG wave behaviour on the reef flat, with a 23% decrease in H_{ig} recorded between C_f =0.001 and C_f = 0.01, compared to a 15% decrease in H_{ss} (Table 1). Overall, the most accurate representation of all wave processes at WG9 (skill > 0.94) was achieved using C_f values between 0.001 and 0.006, combined with $B \geq 0.7$.

Mean skill at WG9 was combined with runup skill to identify input values for C_f and B that provide the best representation of all shoreline processes that are of key interest to coastal management applications. Maximum shoreline skill was associated with B = 0.7 and C_f = 0.005, with consistent outputs and high skill (>0.93) achieved using B = 0.7-1, combined with C_f = 0.004 - 0.007 (Figure 3f). Including R_{max} in the assessment of shoreline skill shifted the location of maximum skill to a lower B value and a slightly higher friction value, compared to maximum skill at WG9. However, the location of maximum skill at C_f = 0.005 and B = 0.7 is within the maximum 5% skill contour for each individual wave process (Figure 3f).

Spectral Wave Transformation

Systematic analysis of model skill revealed that the most accurate representation of all wave processes at the shoreline was achieved using B = 0.7 and C_f = 0.005. However, calibrating the model to achieve the best representation of shoreline wave processes does not necessarily confirm that wave processes across the reef platform were accurately represented. Therefore, wave spectra calculated from numerical model outputs were compared with flume measurements at different wave gauge locations across the reef to further evaluate the accuracy of using B = 0.7 and C_f = 0.005 (Figure 5). Spectra results show a generally strong agreement

between the numerical model and the wave flume at the reef slope (WG5) and across the reef flat (WG7-9). These spectral density plots highlight that the GN model adequately represents the dissipation of SS wave energy across the reef and captures the transfer of energy into long-period IG motions on the reef flat. Further, spectra calculated from GN model outputs show a close match with wave flume spectra across a wide range of incident wave conditions and reef depths that represent high tide, mean tide, low tide and dry reef scenarios (Figure 5).

Benchmark Test 2: Solitary Wave Breaking on a 2D Reef

The HI reef benchmark experiment was simulated using three C_f values (0.001, 0.005, 0.01) combined with three B values (0.4, 0.7, 1), a total of nine model runs. These values encompass the range tested in BM1 and include the combination of $B = 0.7$ and $C_f = 0.005$ that achieved maximum skill at the shoreline. This test requires a solitary wave to pass over a dry reef crest (WG10) and is therefore a fundamental benchmark scenario for wave overtopping processes on coral reefs. Skill values reported in this section are based on comparison of free-surface water level between the numerical model and wave flume.

Model Skill and Sensitivity

All combinations of B and C_f were capable of accurately representing wave shape and timing seaward of the reef crest (WG1-8), with mean skill across the first 8 gauges between 0.96 and 0.99 (Figure 6). Variation in skill throughout the shoaling process was attributed to friction, with maximum skill associated with $C_f = 0.005$ and slightly less skill with higher or lower friction (Figure 6). The value used for B had less influence on offshore skill with $B = 0.4$ and 0.7 producing near identical wave profiles and skill outputs (Figure 6). $B = 1$ was associated with slightly less skill between WG1 and WG8 (Figure 6). The wave face became vertical at the upper reef slope (WG9) before breaking on the reef crest (WG10) between t = 12-15 s (Figure 7). Maximum model skill at WG9 was associated with $C_f = 0.005$, with skill = 0.99

achieved by all B values. Skill at WG9 was slightly lower using C_f = 0.01 and much lower using C_f = 0.001. For all input combinations, model skill decreased between WG9 and WG10 and continued to decrease until WG12, before increasing again at WG13-14 (Figure 6). The highest skill between WG10 and WG12 was consistently achieved using C_f = 0.005, with skill > 0.9 achieved across all wave gauges, regardless of B. Maximum skill in the lagoon was located at WG13 and WG14, with skill > 0.95 achieved using C_f = 0.001 and C_f = 0.005 (Figure 6). The B value associated with maximum skill at each wave gauge in the lagoon was variable, but mean skill between WG9 and WG14 was slightly higher using B = 0.7 (0.948) compared to B = 0.4 (0.945) or B = 1 (0.947). Overall, mean skill across all wave gauges was maximum using C_f = 0.005 and B = 0.7, which is consistent with outputs from BM1.

Model outputs from BM2 show that the shock-capturing GN equations can replicate the highly nonlinear scenario of at 0.75 m solitary wave breaking on an emerged reef crest. Using B = 0.7 and C_f = 0.005, skill was calculated separately for the initial forward propagating wave (t = 0-20 s) and the reflected water level surges (t = 20-60 s). Forward wave propagation and shoaling between WG1 and WG8 was simulated with skill > 0.997, consistent with the numerical wave producing a close visual match to time-series outputs form the wave flume (Figure 7). Numerical representation of wave breaking between WG9 and WG10 was characterised by skill > 0.988, confirming the models ability to represent wave shape, amplitude and timing. A significant decrease in forward propagating skill (0.775) was observed at WG11, where the broken wave initially plunged into the lagoon creating a 0.37 m high spike in water level that lasted for 0.4 s in the wave flume. Numerical outputs at WG11 did create a similar surge event but the timing was slightly delayed, the amplitude was higher (0.45 m) and the spike remained at peak amplitude for longer (0.58 s) compared to flume measurements. Forward propagating model skill increased again between WG12 and WG14, indicating that surge timing, amplitude and shape was reasonably well represented before the wave reflected

off the right boundary at x = 87 m. The reflected bore propagated back across the lagoon between t = 20-30 s, with the reflected signal characterised by skill > 0.9 at all lagoon sensors (WG11 - WG14). Less skill (0.87) was observed at WG10 as the surge passed back over the reef crest, but the timing and amplitude of the modeled reflection remained consistent with flume measurements. Flume data show that a series of short period oscillations were created as the reflected wave propagated into deeper water on the upper reef slope. The reflected signal at WG9 was close to flume measurements (skill = 0.99) showing similar timing and amplitude for the short period waves and longer period surge. Skill decreased slightly as the reflected waves propagated towards WG2 (skill = 0.95) but the water level dynamics associated with the reflected wave propagating seaward were accurately captured in the numerical model (Fig. 7).

Benchmark Test 3: Solitary Wave Breaking on a 3D Reef

The 3D shelf with a conical island experiment from Lynett *et al.* (2011) is one of the only published benchmark tests that provide freely available data for evaluating 2D phase-resolving wave models. Benchmark test 3 was simulated using the same nine combinations of B and C_f that were used in BM2. BM3 is a popular test for fully nonlinear Boussinesq models because it requires numerical solutions for wave dispersion, shoaling, breaking, diffraction, refraction, convergence and overtopping on a dry shoreline. Snapshots of the model free-surface show how the solitary wave washes over and refracts around the conical cone before surging up the beach-face and overtopping the berm (Figure 8).

Model Skill and Sensitivity

Maximum skill for each combination of B and C_f was recorded near the input boundary (WG1 and WG4) where skill varied between 0.95 and 0.97. Model skill decreased along the y = 0 m transect (WGs 1, 2, 3, 7), with skill at WG2 (in front of the conical cone) between 0.85 and 0.87 depending on input values (Figure 9). Numerical model outputs at WG2 show the

timing an shape of the initial wave passing the sensor were close to measurements form the wave flume and suggest that the decrease in model skill is associated with reflections passing over the sensor between t = 20-40 s (Figure 10b). Model outputs directly leeward of the conical cone (WG3) were sensitive to the timing and shape of the initial surges of water passing over and bending around the cone (Figure 10c). Maximum skill at WG3 was 0.88, associated with C_f = 0.001 and B = 0.4, with minimum skill (0.77) associated with C_f = 0.01 and B = 1. Leeward model performance increased further from the cone, with skill at WG7 between 0.86 (C_f = 0.001; B = 1) and 0.90 (C_f = 0.005; B = 0.4). Sensors across the y = 5 m transect (WGs 4, 5, 6, 8) recorded wave processes lateral to the cone and nearly always produced higher skill when compared against gauges on the y = 0 m transect, especially for forward propagating waves (Figure 9). Mean skill across all sensors was highest using C_f = 0.005 combined with B = 0.4 (0.882) or B = 0.7 (0.880). High skill values using B = 0.7 and C_f = 0.005 are consistent with BM1 and BM2 and confirm the use of these values for laboratory scale simulations of wave dynamics on coral reefs.

Velocity

Velocity data were recorded at WG2 and WG3, capturing flow dynamics on seaward and leeward sides of the conical island (Figure 11). In front of the island, WG2 recorded the velocity signal of the steepening solitary wave, with U_x recording a close match to flume measurements using B = 0.7 and C_f = 0.005 (Figure 11a). Numerical outputs at WG2 also recorded a similar U_x signal as reflected water level motions initially surged back over the sensor at t = 7-18 s. Leeward of the island, flume measurements recorded a sharp increase in U_x as the wave surged over the island at t = 7.5 s (Figure 11b). Model results for U_x at WG3 produced the same plunge, followed by a similar trough, between t = 8.5 and 22 s. Modeled U_y data at WG2 and WG3 produced low velocities and did not identify the minor oscillations observed in the flume until t > 22 s (Figure 11d,e). Data from WG10 measured velocity at the

upper reef slope away from the island, with numerical outputs for U_x and the more significant variations in U_y showing a reasonable agreement with flume measurements (Figure 11c,f). Note, skill was not calculated for velocity outputs due to missing sections of data from each of the wave flume sensors.

DISCUSSION

The three benchmark experiments used to evaluate the Popinet (2015) shock capturing GN solver collectively show that the model can skilfully represent surf-zone processes, runup, water level dynamics and overtopping on topographically complex coral reef environments. Of the three benchmark experiments, BM1 provides a comprehensive assessment for applying the model to simulate nonlinear wave transformation processes that contribute to wave driven runup and inundation. BM2 and BM3 provide more detail on how the model represents nonlinear transformations in wave shape and directly test how the GN equations can be applied to simulate wave overtopping scenarios. Physical phenomenon that contribute to wave runup and inundation on atoll islands include: SS waves, IG waves and setup (Merrifield *et al.*, 2014). Field measurements demonstrate how each of these processes respond differently to incident wave conditions and reef depth (Becker, Merrifield, and Ford, 2014; Ford, Becker, and Merrifield, 2013; Kench and Brander, 2006; Pomeroy *et al.*, 2012). Further, these processes influence the behaviour of each other, complicating a conceptual understanding of how environmental conditions influence runup on reef fringed coastlines. Recent developments in numerical modeling (*e.g.* Popinet, 2015; Roeber and Cheung, 2012b; Su, Ma, and Hsu, 2015) allow these nonlinear interactions to be simulated under controlled boundary conditions, and provide a unique tool for exploring how physical processes will respond to environmental change. However, appropriate and efficient use of these new modeling techniques relies on a comprehensive understanding of how numerical outputs are influenced by parameters that are typically used for model 'tuning' and calibration (Oreskes *et al.*, 1994). Systematic analysis

from BM1 revealed how SS attenuation, IG transmission, setup and runup each exhibit individual sensitivity to breaking and friction parameters. Therefore, a combined assessment of all parameters is required to achieve a realistic representation of processes that impact the shoreline. In general, outputs were more sensitive to the fiction coefficient (C_f) than to the slope threshold used for locally removing dispersion (B). However, the model was highly sensitive to B = 0.4 (21.8°) because wave breaking was initiated to far offshore. Wave setup was significantly over-predicted using B = 0.4 which meant that IG waves were not sufficiently dissipated by friction processes on the reef flat. Model outputs observed minimal sensitivity and maximum skill using slope thresholds between B = 0.7 (35°) and B = 1.2 (~50°). These findings are consistent with Buckley, Lowe, and Hansen (2014) where a breaking slope of ~55° was found to give the best prediction of UM measurements when using the nonlinear phase-resolving model SWASH (SWASH default is 25°). Using a high breaking slope can be explained physically in this context because of the steep sloping fore-reef on coral reefs typically produces plunging breakers.

Higher friction values were associated with both SS and IG waves being under-predicted at the shoreline. IG waves were highly sensitive to friction, with H_{ig} over-predicted at WG9 using low friction but dramatically under-predicted using high friction. However, skilful predictions for IG wave height were achieved using a C_f range between 0.002 and 0.008. Model results highlight the role of friction as a primary control for low frequency wave behaviour on coral reefs. Wave setup was consistently well predicted, with minimal sensitivity to friction, unless B = 0.4 was used. Accounting for R_{max} added an additional level of complexity when trying to achieve an accurate prediction of all processes at the shoreline. Maximum runup was highly sensitive to SS and IG dynamics, leading to over-predicted runup with low friction and under-predicted runup using high friction. However, skilful predictions were achieved using moderate friction (0.005 to 0.01) and any B value above 0.6. The best

representation of all processes was found using $C_f = 0.005$ and $B = 0.7$. These same input values were capable of skilfully replicating solitary wave transformation on complex 2D and 3D reef structures, with a slight decrease in skill observed when using the model in 2DH (two horizontal dimensions). Collectively, the three benchmark scenarios show that the GN model is capable of simulating the range of wave frequencies and nonlinear dynamics associated with wave transformation on coral reef systems.

CONCLUSIONS

A benefit of fully nonlinear free-surface models is that any feedbacks between different frequency wave processes are directly resolved (Shimozono *et al.*, 2015). For example, the attenuation of irregular SS waves is associated with the formation of IG motions and setup that in turn influence the transmission of broken and reformed SS waves across the reef flat. These feedbacks are critical for accurately representing the range of processes that promote elevated sea-level and coastal flooding, as recently highlighted by Roeber and Bricker (2015). However, the interlinked nature of these models also means that the sensitivity of each process needs to be carefully understood before being applied to real world scenarios. Simulations presented here are the first step towards applying the GN solution to study the complex interplay of processes associated with wave transformation on coral reef coastlines. Results suggest that the combination of weakly dispersive Green-Naghdi equations and nonlinear shallow water equations implemented in Popinet (2015) and other model packages have significant potential for simulating detailed wave processes on reef environments. Consequently, this type of modeling can become a powerful research tool to explore wave dynamics on reef systems in context of future environmental change.

ACKNOWLEDGEMENTS

This research was part of a PhD theses completed by Edward Beetham at the School of Environment, University of Auckland (UoA) and was supported by a UoA Doctoral Scholarship.

LITERATURE CITED

Becker, J.; Merrifield, M., and Ford, M., 2014. Water Level Effects on Breaking Wave Setup for Pacific Island Fringing Reefs. *Journal of Geophysical Research: Oceans,* 119 (2), 914-932.

Beetham, E P.; Kench, P S.; O'Callaghan, J., and Popinet, S., 2016. Wave Transformation and Shoreline Water Level on Funafuti Atoll, Tuvalu. *Journal of Geophysical Research: Oceans,* 121 (1), 311-326.

Bonneton, P.; Barthelemy, E.; Chazel, F.; Cienfuegos, R.; Lannes, D.; Marche, F., and Tissier, M., 2011a. Recent Advances in Serre-Green Naghdi Modelling for Wave Transformation, Breaking and Runup Processes. *European Journal of Mechanics B-Fluids,* 30 (6), 589-597.

Bonneton, P.; Chazel, F.; Lannes, D.; Marche, F., and Tissier, M., 2011b. A Splitting Approach for the Fully Nonlinear and Weakly Dispersive Green–Naghdi Model. *Journal of Computational Physics*, 230 (4), 1479-1498.

Buckley, M.; Lowe, R., and Hansen, J., 2014. Evaluation of Nearshore Wave Models in Steep Reef Environments. *Ocean Dynamics,* 64 (6), 847-862.

Cheriton, O.; Storlazzi, C D., and Rosenberger, K., 2016. Observations of Wave Transformation over a Fringing Coral Reef and the Importance of Low-Frequency Waves and Offshore Water Levels to Runup, Overwash, and Coastal Flooding. *Journal of Geophysical Research: Oceans,* 121 (5), 3121-3140.

Demirbilek, Z., and Nwogu, O G., 2007. *Boussinesq Modeling of Wave Propagation and Runup over Fringing Coral Reefs, Model Evaluation Report. U.S. Army Engineer Research and Development Center, 101p.*

Demirbilek, Z.; Nwogu, O G., and Ward, D L., 2007. *Laboratory Study of Wind Effect on Runup over Fringing Reefs. Report 1. Data Report. U.S. Army Engineer Research and Development Center, 70p.*

Fang, K.; Liu, Z., and Zou, Z., 2016. Fully Nonlinear Modeling Wave Transformation over Fringing Reefs Using Shock-Capturing Boussinesq Model. *Journal of Coastal Research,* 32 (1), 164-171.

Fang, K.; Zou, Z.; Dong, P.; Liu, Z.; Gui, Q., and Yin, J., 2013. An Efficient Shock Capturing Algorithm to the Extended Boussinesq Wave Equations. *Applied Ocean Research,* 43, 11-20.

Ferrario, F.; Beck, M W.; Storlazzi, C D.; Micheli, F.; Shepard, C C., and Airoldi, L., 2014. The Effectiveness of Coral Reefs for Coastal Hazard Risk Reduction and Adaptation. *Nature Communications*, 5, doi: 10.1038/ncomms4794.

Filipot, J-F., and Cheung, K F. 2012., Spectral Wave Modeling in Fringing Reef Environments. *Coastal Engineering*, 67 (0), 67-79.

Ford, M.; Becker, J., and Merrifield, M., 2013. Reef Flat Wave Processes and Excavation Pits: Observations and Implications for Majuro Atoll, Marshall Islands. *Journal of Coastal Research,* 29 (3), 545-554.

Huntley, D A., 2013. Waves. In*:* Sherman, D J, ed. *Coastal Geomorphology*, Academic Press, San Diego, pp. 39-73.

Kench, P S., and Brander, R W., 2006. Wave Processes on Coral Reef Flats: Implications for Reef Geomorphology Using Australian Case Studies. *Journal of Coastal Research,* 22 (1), 209-223.

Lannes, D., and Marche, F., 2015. A New Class of Fully Nonlinear and Weakly Dispersive Green–Naghdi Models for Efficient 2D Simulations. *Journal of Computational Physics,* 282, 238-268.

Lowe, R J.; Falter, J L.; Monismith, S G., and Atkinson, M J., 2009. Wave-Driven Circulation of a Coastal Reef-Lagoon System. *Journal of Physical Oceanography,* 39 (4), 873-893.

Lynett, P J.; Swigler, D.; Son, S.; Bryant, D., and Socolofsky, S., 2011. Experimental Study of Solitary Wave Evolution over a 3D Shallow Shelf. *Proceedings of the 32nd International Conference on Coastal Engineering* (Shanghai, China), doi: https://doi.org/10.9753/icce.v32.currents.1.

Merrifield, M.; Becker, J.; Ford, M., and Yao, Y., 2014. Observations and Estimates of Wave-Driven Water Level Extremes at the Marshall Islands. *Geophysical Research Letters,* 41 (20), 7245-7253.

NTHMP Contributers., 2012. *Proceedings and Results of the 2011 National Tsunami and Hazard Mitigation (NTHMP) Model Benchmarking Workshop, NOAA Special Report*, Boulder, Colorado, U. S., 436p.

Nwogu, O., and Demirbilek, Z., 2010. Infragravity Wave Motions and Runup over Shallow Fringing Reefs. *Journal of Waterway, Port, Coastal, and Ocean Engineering,* 136 (6), 295-305.

Oreskes, N.; Shraderfrechette, K., and Belitz, K., 1994. Verification, Validation, and Confirmation of Numerical-Models in the Earth-Sciences. *Science,* 263 (5147), 641-646.

Péquignet, A C.; Becker, J M., and Merrifield, M A., 2014. Energy Transfer between Wind Waves and Low-Frequency Oscillations on a Fringing Reef, Ipan, Guam. *Journal of Geophysical Research: Oceans,* 119 (10), 6709-6724.

Pomeroy, A.; Lowe, R.; Symonds, G.; Van Dongeren, A., and Moore, C., 2012. The Dynamics of Infragravity Wave Transformation over a Fringing Reef. *Journal of Geophysical Research: Oceans,* 117, C11022.

Popinet, S., 2014. *A Solver for the Green-Naghdi Equations*, http://www.basilisk.fr/src/green-naghdi.h.

Popinet, S., 2015. A Quadtree-Adaptive Multigrid Solver for the Serre–Green–Naghdi Equations. *Journal of Computational Physics,* 302, 336-358.

Reyns, J.; Ap van Dongeren, D R.; Lowe, R.; Falter, J., and Boruff, B., 2013. Vulnerability of Coral Reef Protected Coastlines in a Changing Environment. *White Paper: A report to the Asian Development Bank within the framework of the ADB - UNESCO - IHE Knowledge Partnership,* Department of Water Science and Engineering UNESCO - IHE Institute for Water Education, pp. 100.

Roeber, V., and Bricker, J D., 2015. Destructive Tsunami-Like Wave Generated by Surf Beat over a Coral Reef During Typhoon Haiyan. *Nature Communications,* 6, doi: 10.1038/ncomms8854.

Roeber, V., and Cheung, K F., 2012a. BOSZ *In*: Program, NTHMP (ed.) *Proceedings and Results of the 2011 National Tsunami and Hazard Mitigation (NTHMP) Model Benchmarking Workshop, NOAA Special Report*, Boulder, Colorado, U. S., 361-406.

610 Roeber, V., and Cheung, K F., 2012b. Boussinesq-Type Model for Energetic Breaking Waves
611 in Fringing Reef Environments. *Coastal Engineering,* 70, 1-20.
612 Sheremet, A.; Kaihatu, J M.; Su, S F.; Smith, E R., and Smith, J M., 2011. Modeling of
613 Nonlinear Wave Propagation over Fringing Reefs. *Coastal Engineering,* 58 (12), 1125-
614 1137.
615 Shi, F.; Kirby, J T.; Harris, J C.; Geiman, J D., and Grilli, S T., 2012. A High-Order Adaptive
616 Time-Stepping Tvd Solver for Boussinesq Modeling of Breaking Waves and Coastal
617 Inundation. *Ocean Modelling,* 43, 36-51.
618 Shimozono, T.; Tajima, Y.; Kennedy, A B.; Nobuoka, H.; Sasaki, J., and Sato, S., 2015.
619 Combined Infragravity Wave and Sea-Swell Runup over Fringing Reefs by Super
620 Typhoon Haiyan. *Journal of Geophysical Research: Oceans,* 120 (6), 4463-4486.
621 Storlazzi, C D.; Elias, E P L., and Berkowitz, P., 2015. Many Atolls May Be Uninhabitable
622 within Decades Due to Climate Change. *Scientific Reports,* 5, doi: 10.1038/srep14546.
623 Storlazzi, C D.; Ogston, A S.; Bothner, M H.; Field, M E., and Presto, M K., 2004. Wave- and
624 Tidally-Driven Flow and Sediment Flux across a Fringing Coral Reef: Southern
625 Molokai, Hawaii. *Continental Shelf Research,* 24 (12), 1397-1419.
626 Su, S-F.; Ma, G., and Hsu, T-W., 2015. Boussinesq Modeling of Spatial Variability of
627 Infragravity Waves on Fringing Reefs. *Ocean Engineering,* 101 (0), 78-92.
628 Su, S-F.; Sheremet, A., and Smith, J M., 2011. Parametric Wave-Breaking on Steep Reefs.
629 *Proceedings of the 32nd International Conference on Coastal Engineering* (Shanghai,
630 China), doi: https://doi.org/10.9753/icce.v32.waves.16.
631 Tissier, M.; Bonneton, P.; Marche, F.; Chazel, F., and Lannes, D., 2012a. A New Approach to
632 Handle Wave Breaking in Fully Non-Linear Boussinesq Models. *Coastal Engineering,*
633 67 (0), 54-66.
634 Tissier, M.; Bonneton, P.; Ruessink, B.; Marche, F.; Chazel, F., and Lannes, D., 2012b. Fully
635 Nonlinear Boussinesq-Type Modelling of Infragravity Wave Transformation over a
636 Low-Sloping Beach. *Proceedings of the 33rd International Conference on Coastal*
637 *Engineering* (Santander, Spain), doi: https://doi.org/10.9753/icce.v33.currents.28.
638 Vetter, O.; Becker, J M.; Merrifield, M A.; Péquignet, A C.; Aucan, J.; Boc, S J., and Pollock,
639 C E., 2010. Wave Setup over a Pacific Island Fringing Reef. *Journal of Geophysical*
640 *Research: Oceans,* 115, C12066.
641 Yamazaki, Y.; Cheung, K F.; Kowalik, Z.; Lay, T., and Pawlak, G., 2012. NEOWAVE. *In*:
642 Program, NTHMP (ed.) *Proceedings and Results of the 2011 National Tsunami and*
643 *Hazard Mitigation (NTHMP) Model Benchmarking Workshop, NOAA Special Report,*
644 Boulder, Colorado, U. S., 239-302.
645 Zijlema, M., 2012. Modelling Wave Transformation across a Fringing Reef Using SWASH.
646 *Proceedings of the 33rd International Conference on Coastal Engineering*
647 (Santander, Spain), doi: https://doi.org/10.9753/icce.v33.currents.26.

Tables

Table 1. *Summary of numerical model skill and sensitivity when compared to flume measurements of SS wave height, IG wave height, setup and runup at the shoreline. Values assigned to the WG9 column represent the mean skill across all wave process (H_{ss}, H_{ig} and setup) at the shoreline and shoreline skill is the average skill from all wave processes at WG9 and runup. A statistical summary of model skill is first presented, based on all simulations, to provide an indication of how variable outputs are when inputs are modified. To quantify model sensitivity, the percent difference between minimum and maximum values were calculated for all C_f values, all B values and the higher and lower range of C_f and B values. B and Cf values associated with maximum skill are presented as recommended values for predicting each wave process. The range of B and C_f combinations that can be used while maintaining model skill within 5% of maximum skill are shown as the minimum and maximum B and C_f values that make up this range.*

	H_{ss}	H_{ig}	Setup	WG9 (Mean)	Runup	Shoreline
Model skill						
Maximum	0.901	0.977	0.988	0.949	0.944	0.936
Max 5% range	0.856	0.928	0.938	0.902	0.896	0.889
Mean	0.858	0.887	0.973	0.906	0.798	0.879
SD	0.057	0.141	0.025	0.065	0.14	0.07
Minimum	0.668	0.419	0.902	0.692	0.419	0.664
Output sensitivity: range between minimum and maximum values						
B (0.4-1.2)	11.9%	16.7%	15.9%	14.8%	20.0%	16.1%
B (0.4-0.7)	11.1%	16.7%	15.1%	14.3%	20.0%	15.7%
B (0.7-1.2)	0.9%	1.7%	1.0%	1.2%	1.2%	1.2%
C_f (0.001-0.01)	14.6%	23.2%	0.7%	12.8%	30.1%	17.2%
C_f (0.001-0.005)	7.6%	12.2%	0.3%	6.7%	19.4%	9.9%
C_f (0.006-0.01)	6.1%	10.0%	0.3%	5.5%	10.8%	6.8%
Recommended B values						
Maximum skill	0.4	0.5	1	0.8	0.7	0.7
5% range: minimum	0.4	0.5	0.5	0.5	0.6	0.6
5% range: maximum	1.2	1.2	1.2	1.2	1.2	1.2
Recommended C_f values						
Maximum skill	0.004	0.006	0.0001	0.003	0.01	0.005
5% minimum	0.0001	0.002	0.0001	0.0001	0.005	0.002
5% maximum	0.008	0.008	0.04	0.01	0.01	0.01

Figure Captions

Figure 1. Example of model capability for simulating irregular wave transformation (H_s = 2.6 m, T_s = 10.5 s) on an idealised coral reef (h_r = 1 m) with a 1:6 fore-reef slope and 1:14 beach slope. (a) Across reef variations in free-surface water level (wave profile), mean water level (setup) and maximum water level. (b-e) Water level time-series outputs at different locations across the model domain showing the raw signal and the low pass filtered (0.04 Hz) infragravity wave signal.

Figure 2. Model bathymetry for each benchmark test showing the location of wave gauge (WG) sensors used to compare numerically modeled outputs with measured wave basin data. (a) Benchmark 1 is the idealised Guam reef from a series of flume experiments undertaken in the University of Michigan wave laboratory (Demirbilek, Nwogu, and Ward, 2007). (b) Benchmark 2 is the Hawaii Reef (HI reef) bathymetry used in the O.H. Hinsdale Wave Flume (Roeber and Cheung, 2012b). (c) Benchmark 3 uses the model in 2D with a complex reef bathymetry that has a steep slope, a triangular shelf and a conical island (Lynett *et al.*, 2011).

Figure 3. Model skill contour lines are presented in grey to show how B and C_f values influence the accuracy of wave processes at the shoreline, individually and collectively, from BM1. Shoreline skill at WG9 is presented for (a) SS wave height, (b) IG wave height and (c) setup at the shoreline. (d) Mean skill at WG9 is the average of individual skill values for H_{ss}, H_{ig} and $\overline{\eta}$ at the shoreline. (e) R_{max} skill. (f) Shoreline skill as the average skill from H_{ss}, H_{ig}, $\overline{\eta}$ at WG9 and R_{max}. Maximum skill is identified with a black marker and the associated C_f and B value is written inside each plot. Black contour lines indicate C_f and B combinations that produce a skill value within 5% of the maximum skill. Note, the x-axis is a log scale.

Figure 4. (a-i) Measured (wave flume) outputs for SS wave height (H_{ss}), IG wave height (H_{ig}) and wave setup are compared to numerical model outputs using a selection of different C_f and B values for the 15 UM test scenarios. (j-r) Numerical model outputs for runup elevation are compared to wave flume measurements for the same selection of B and C_f values. The dashed line represents a perfect fit (y = x) and can be used to visually identify how close model outputs are to flume measurements. Skill values written in plots a-i represent mean skill at WG9, with runup skill presented in plots j-r.

Figure 5. Wave spectra calculated from the GN model outputs using C_f = 0.005 and B = 0.7 (black) are compared to wave spectra calculated from wave flume data (grey) at the upper reef

slope (WG5), outer reef flat (EG7), central reef flat (WG8) and the shoreline (WG9). Eight of the fifteen UM scenarios are presented to show how the model behaves under different incident wave conditions under high tide (rows 1-2), mean tide (rows 3-4), low tide (rows 5-6) and dry reef (rows 7-8) conditions. Note that the x and y axes are both log scale.

Figure 6. Across reef variation in free-surface water level skill at the 14 wave gauge locations from BM2, using different B values (represented using different line symbols) and friction values. (a) C_f = 0.001, (b) C_f = 0.05 and (c) C_f = 0.01. (d) Wave flume bathymetry and wave gauge locations are presented to highlight the spatial influence variation in skill across the reef.

Figure 7. (a-l) Free-surface water level across the model domain at different time snapshots are presented to show wave propagation, breaking and plunging processes from the GN model (black line), using C_f = 0.005 and B = 0.7, compared with wave flume measurements at each wave gauge location (grey circles). (m-x) Comparison of time-series water level measurements from the GN model (black) and wave flume (grey) using B = 0.7 and C_f = 0.005.

Figure 8. Snapshots of free-surface water level at different times during the 3D shelf simulation for BM3, using B = 0.7 and C_f = 0.005.

Figure 9. Comparison of model skill for representing free-surface water level at different wave gauge locations, relative to distance from the incident boundary for the y = 0 m (WGs 1, 2, 3, 7), y = 5 m (WGs 4, 5, 6, 8) at y = 10 m (WG9) transect, for each combination of C_f and B. Mean skill value across all WG locations is presented inside each subplot.

Figure 10. Time-series outputs for free-surface water level at each wave gauge location from the GN model using C_f = 0.005 and B = 0.7 (black) are compared to water level measurements from the wave flume (grey).

Figure 11. Modeled velocity outputs from the GN model using C_f = 0.005 and B = 0.7 (black) are compared to wave flume measurements (grey) at WG2 (seaward of conical cone), WG3 (leeward of conical cone) and WG10 (lateral to conical cone).

Figure 1

Click here to download Figure Fig 01 Model sketch annotated.tif

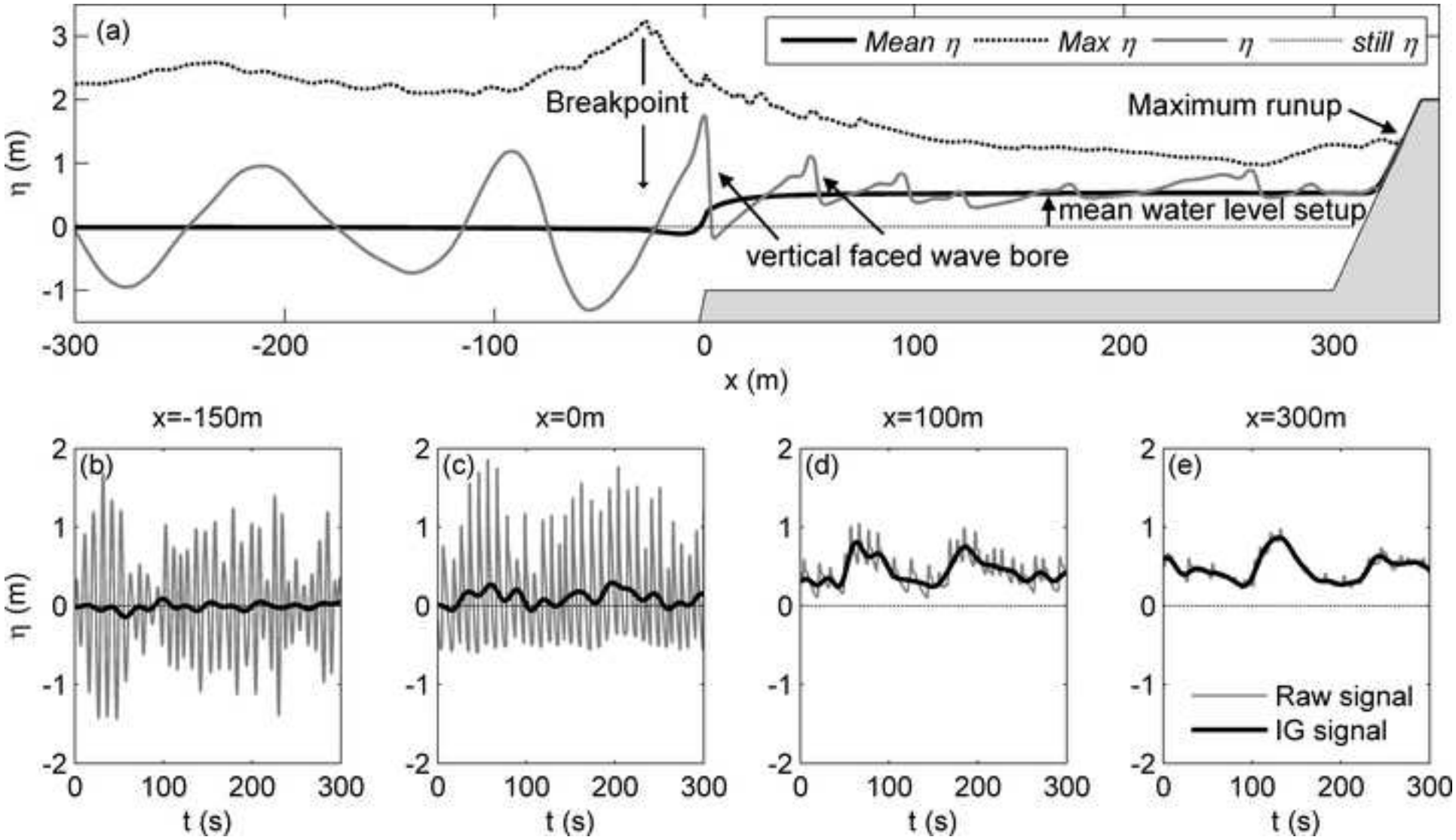

Figure 2

Click here to download Figure Fig 02 Bathy PS.tif

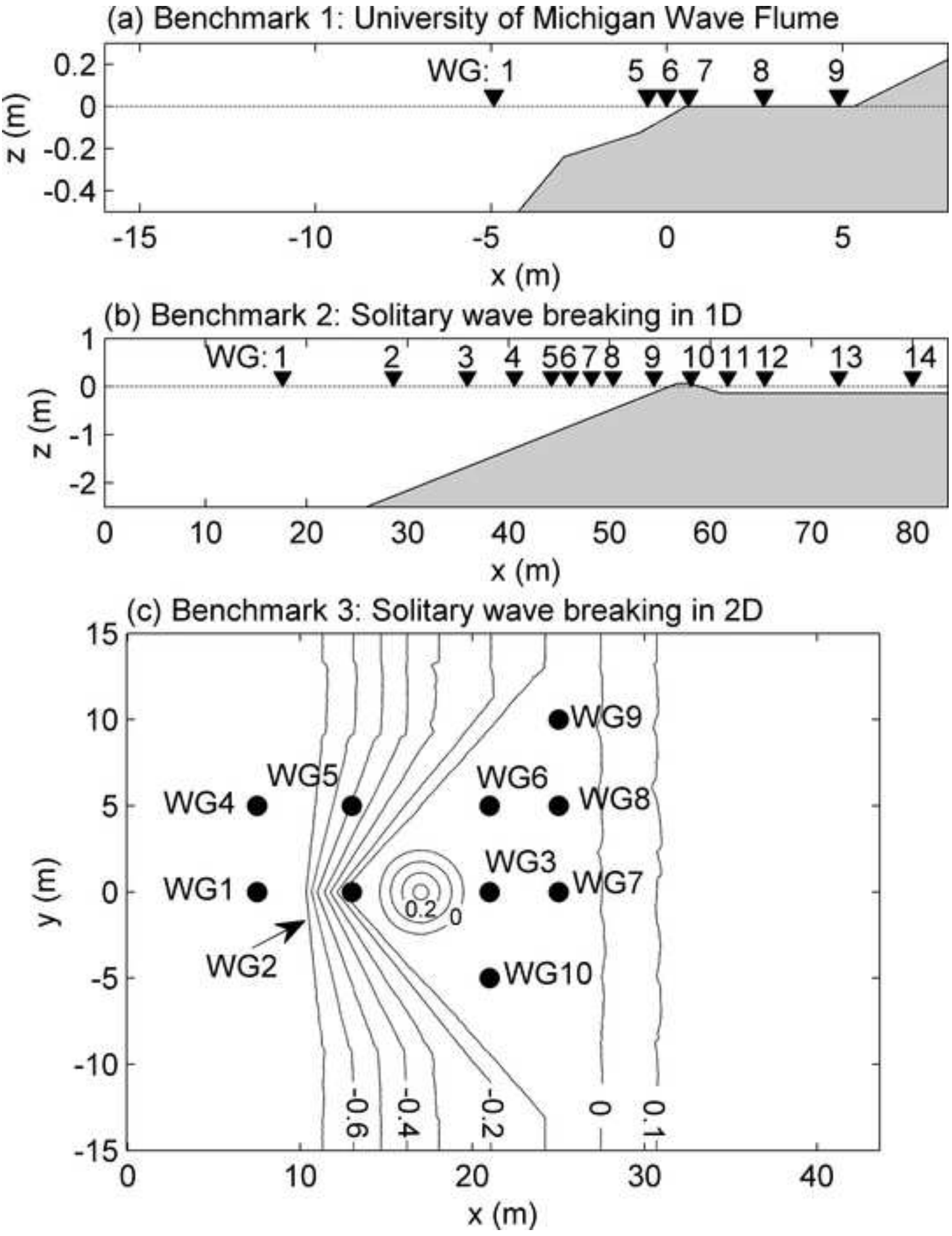

Figure 3

Click here to download Figure Fig 03 Skill Contours PS.tif

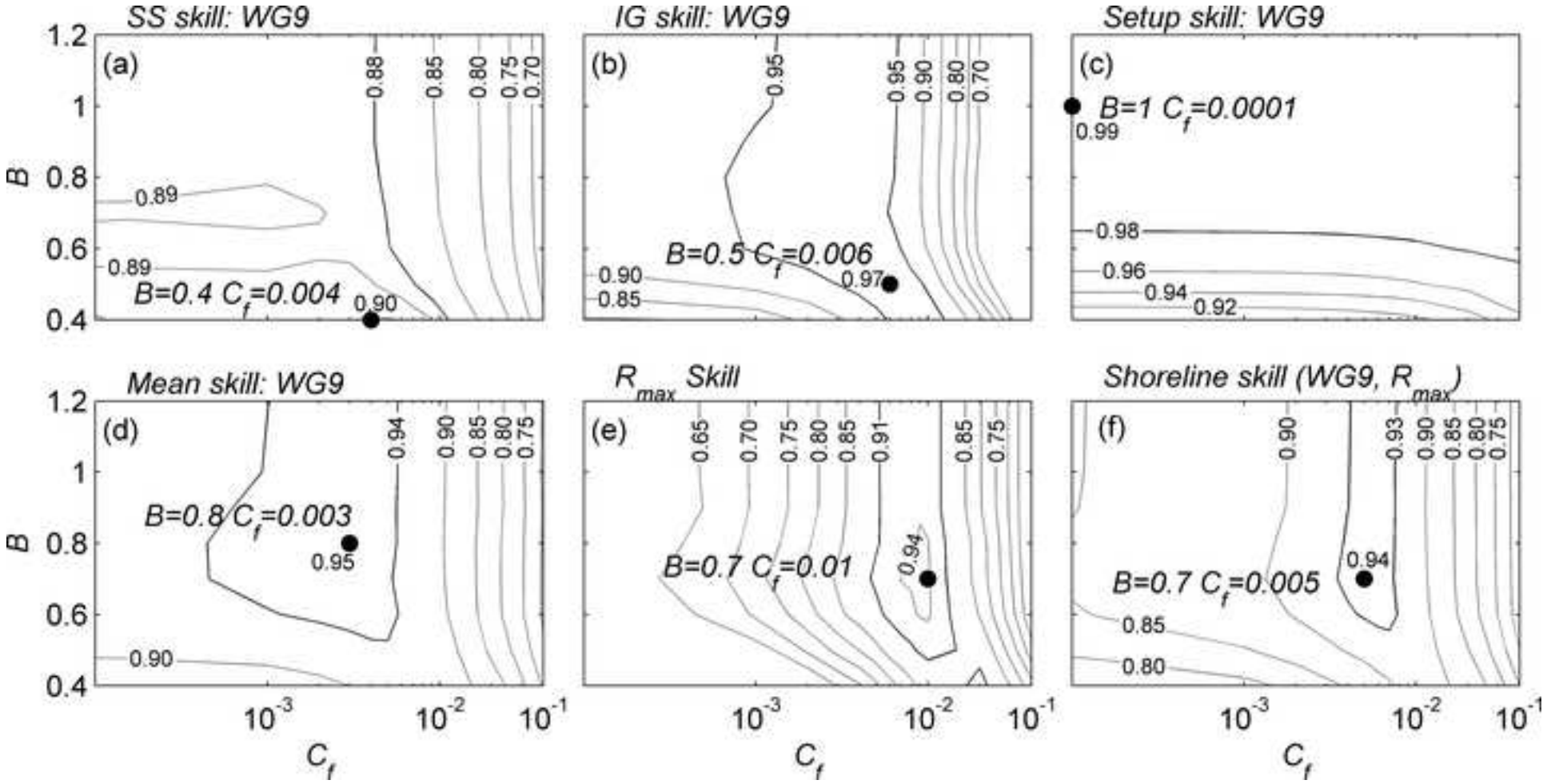

Figure 4

Click here to download Figure Fig 04 BM1 Scatters.tif

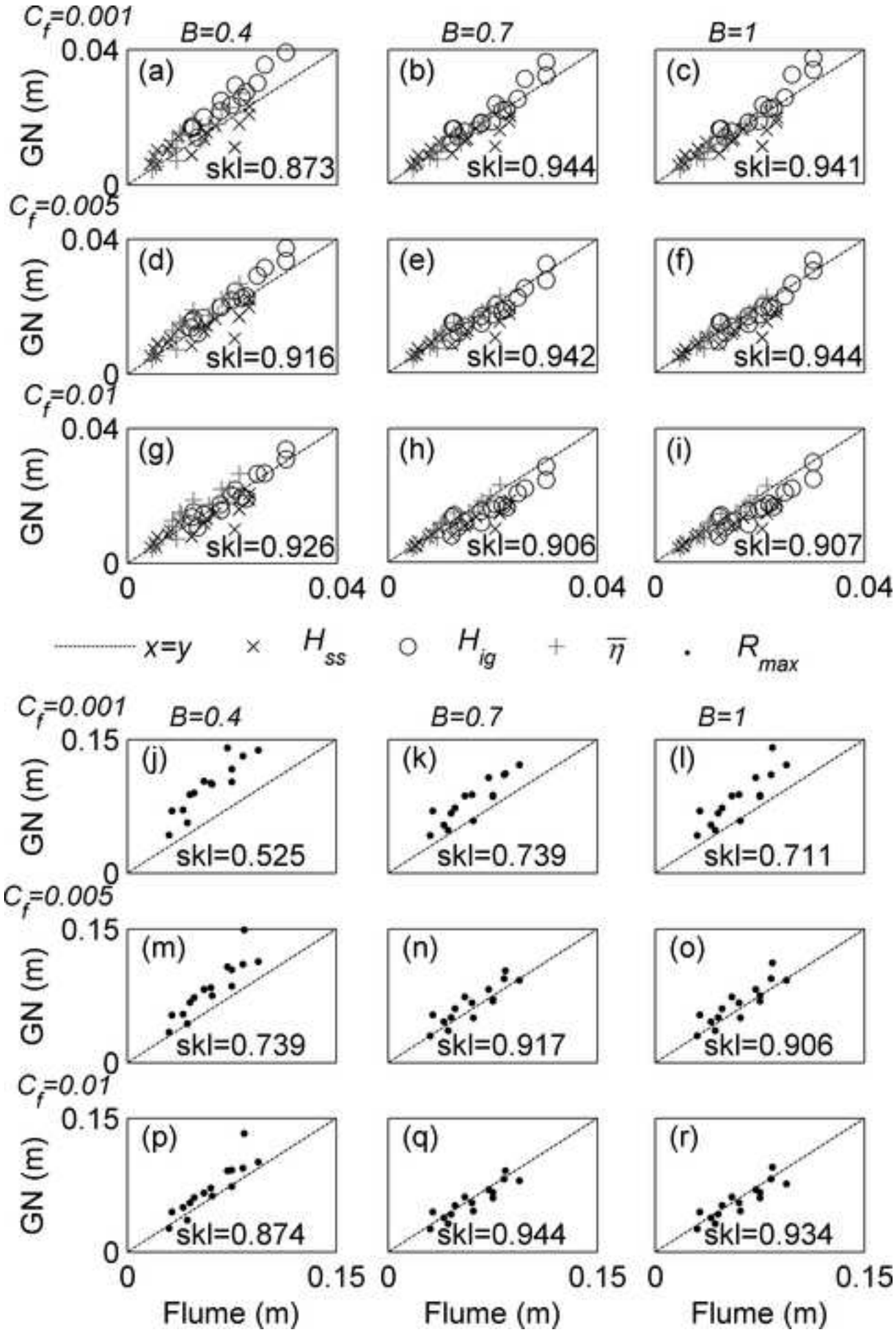

Figure 5

Click here to download Figure Fig 05 BM1 Spectra.tif

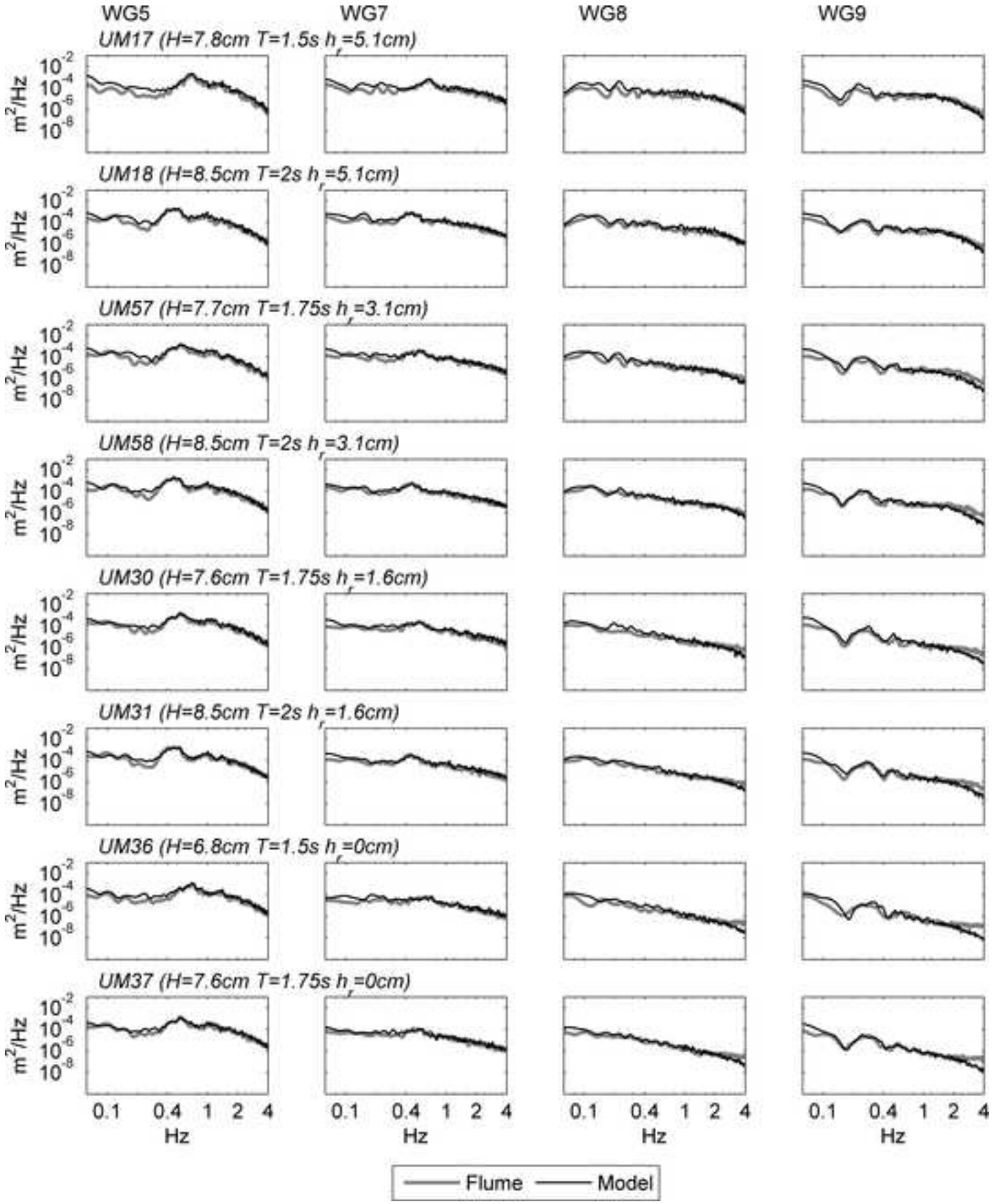

Figure 6

Click here to download Figure Fig 06 BM2 Skill.tif

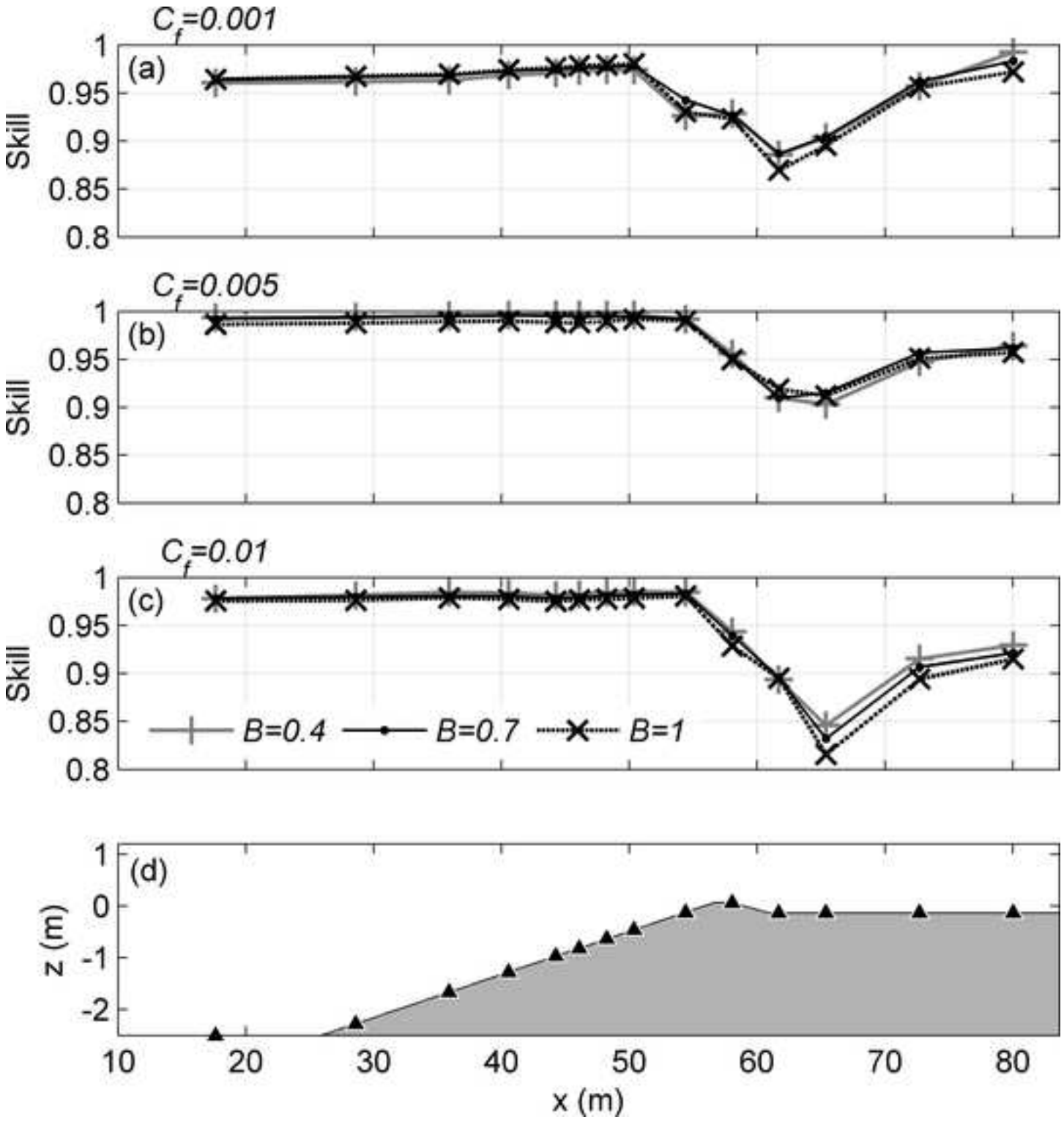

Figure 7

Click here to download Figure Fig 07 free-surf B07.tif

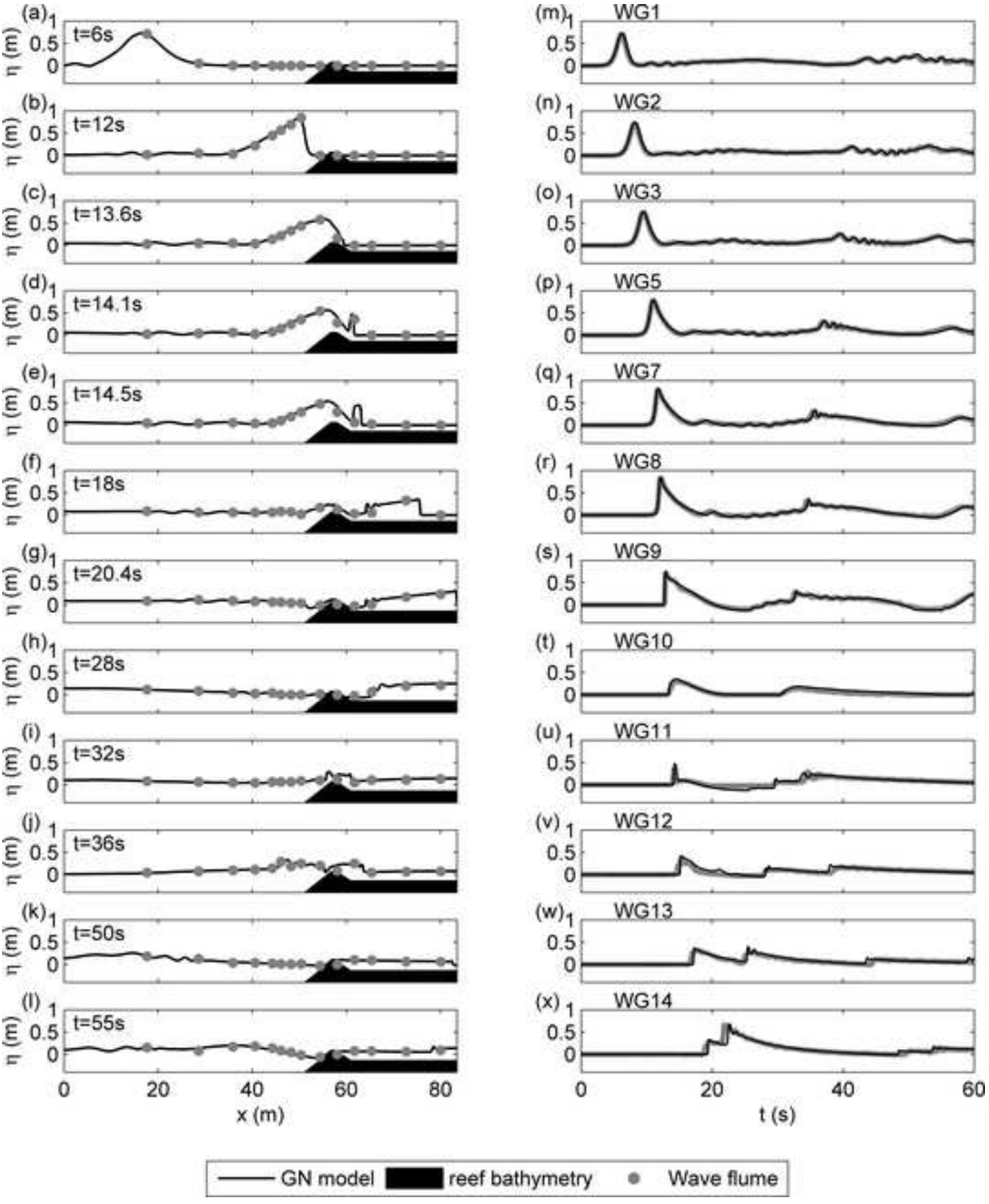

Figure 8

Click here to download Figure Fig 08 BM3 surf PS.tif

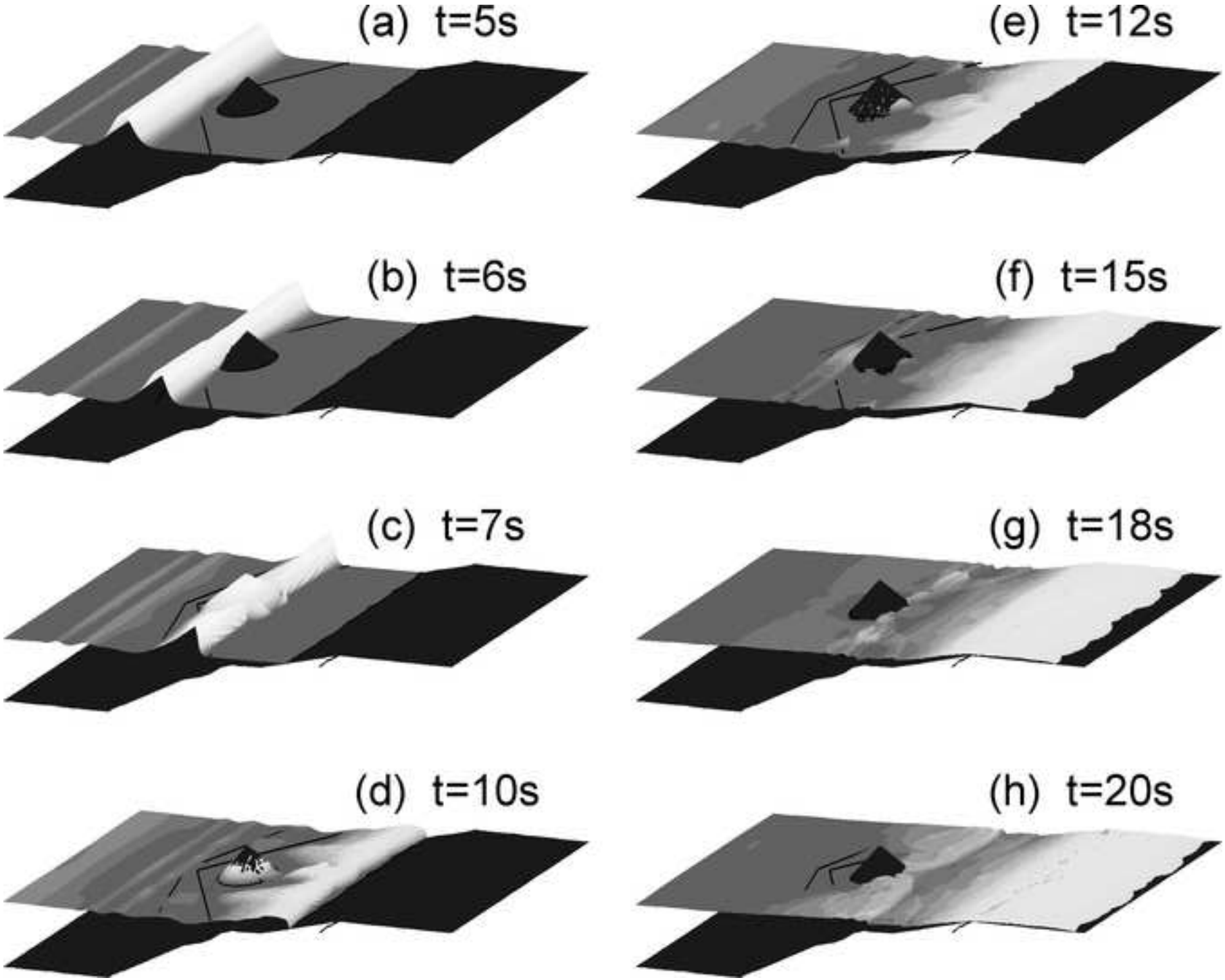

Figure 9

Click here to download Figure Fig 09 Skill.tif

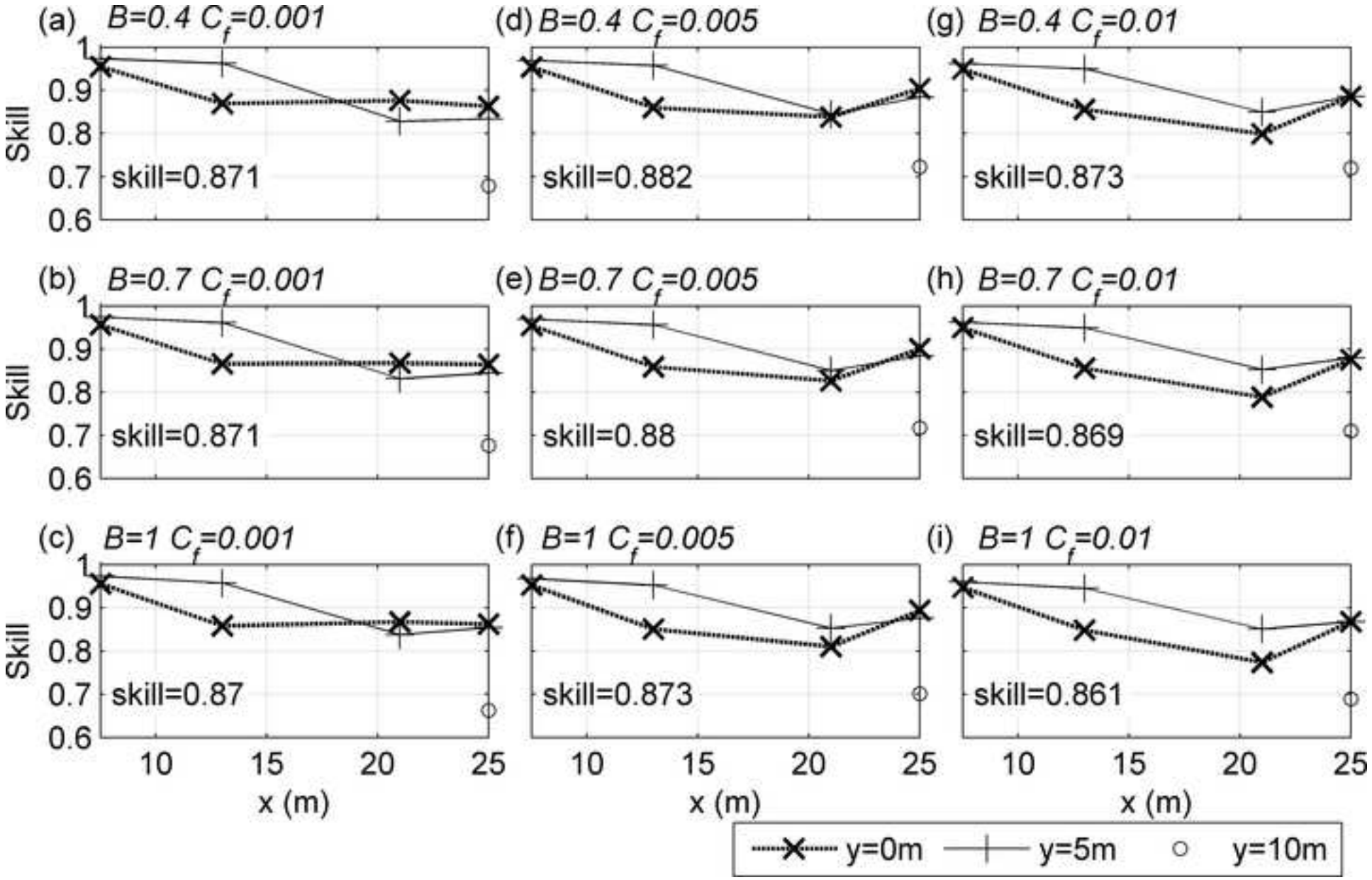

Figure 10

Click here to download Figure Fig 10 free time-series.tif

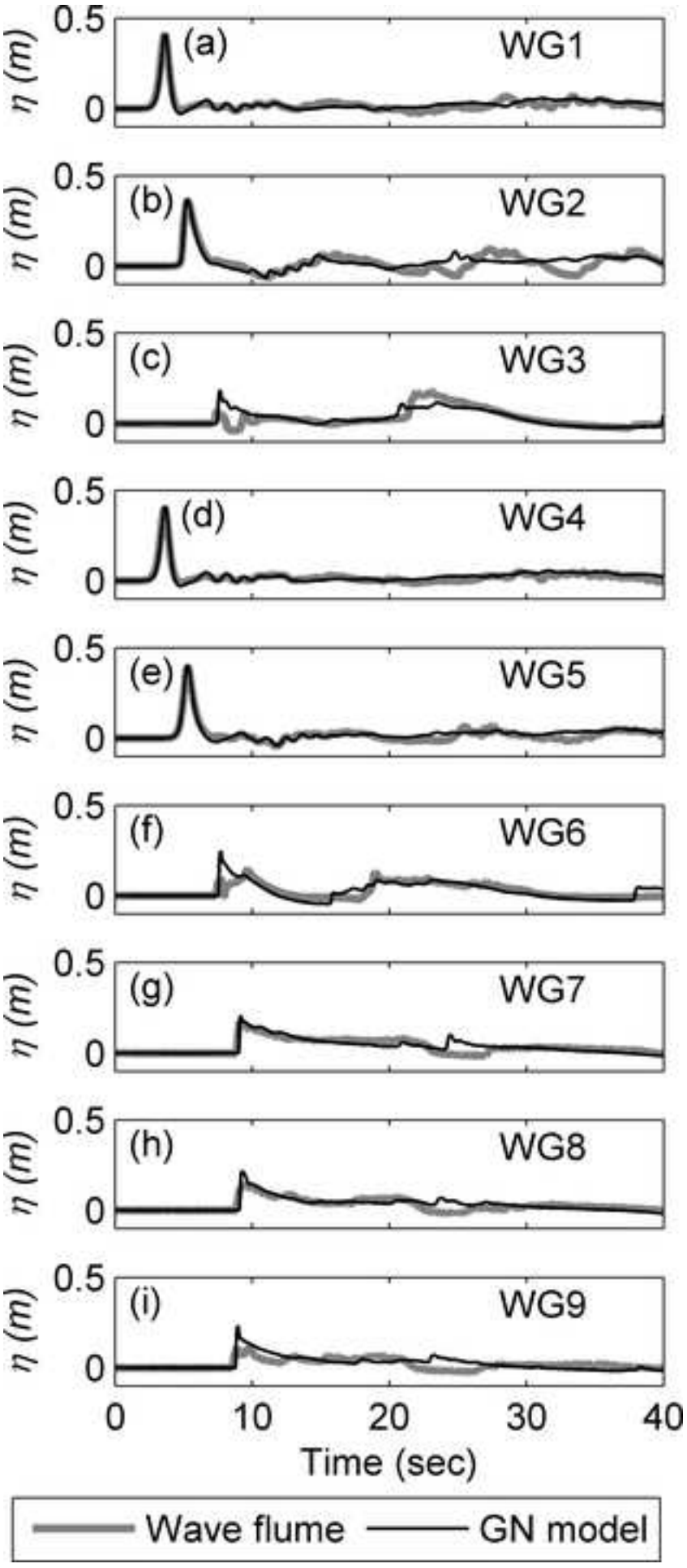

Figure 11

Click here to download Figure Fig 11 Vel.tif